

Review of Traction and Braking Control for Electric Vehicle

Hiroshi Fujimoto, Junya Amada and Kenta Maeda

The University of Tokyo

Graduate School of Frontier Sciences

5-1-5, Kashiwanoha, Kashiwa, Chiba 227-8561, Japan

E-mail: fujimoto@k.u-tokyo.ac.jp, amada@hflab.k.u-tokyo.ac.jp, maeda@hflab.k.u-tokyo.ac.jp

Abstract—Electric vehicles (EVs) have attracted considerable interest because they have zero emissions. Moreover, EVs are considered promising from the viewpoint of vehicle motion control because electric motors have a quick and measurable torque response. Our research group has proposed many motion control methods for EVs. In this paper, our studies on traction and braking control methods are reviewed. These methods can prevent slipping on slippery roads by means of slip ratio estimation and control. Moreover, we have also developed a driving force control method that can control the driving or braking force directly even on an arbitrary μ road. The performance of these methods is explained through numerous simulation and experimental results.

I. INTRODUCTION

In recent times, environmental problems such as global warming, fossil fuel exhaustion, and air pollution have assumed serious proportions. In this light, electric vehicles (EVs) have attracted considerable interest because they have zero emissions. Furthermore, EVs offer various advantages compared to internal combustion engine vehicles (ICEVs)[1]. These advantages can be summarized as follows.

1) Quick torque response

Electric motors have a torque response of the order of a few milliseconds, whereas ICEVs have a torque response of 100–500 ms. Therefore, electric motors enable quick feedback control; furthermore, they can also generate regenerative braking torque.

2) Motor torque can be measured easily

The output torque of ICEVs is difficult to measure accurately. In contrast, that of electric motors can easily be measured accurately from the current.

3) Individual wheels

Owing to the development of in-wheel motor technologies, electric motors can be installed in each wheel of an EV. The individual control of each motor can improve vehicle stability.

Various vehicle motion control methods have been proposed to exploit the advantages offered by these motors[2]–[3]. For example, traction control methods have been proposed to realize safe driving on slippery roads[4]–[6].

In this paper, we review our recent studies on traction and braking control methods, e.g., slip ratio estimation and control method without using vehicle velocity[7], driving



Fig. 1. Experimental vehicle.

Table I
SPECIFICATIONS OF VEHICLE.

Vehicle mass (M)	870 [kg]
Wheel base (l)	1.7 [m]
Tread base (d_f, d_r)	1.3 [m]
Wheel radius (r)	0.302 [m]
Inertia of front wheel J_f	1.24 [kgm ²]
Inertia of rear wheel J_r	1.26 [kgm ²]

force control (DFC) based on wheel velocity control[8], driving force distribution method for instantaneous slippery roads[8], and direct driving force control (DDFC) based on driving stiffness estimation[9].

II. EXPERIMENTAL VEHICLE

To verify the proposed control algorithm, an EV called "FPEV2-Kanon," which was originally developed in our laboratory, is used as a test vehicle. Fig. 1 shows a photograph of FPEV2-Kanon and Fig. 2, its configuration.

In this vehicle, outer-rotor-type in-wheel motors made by Toyo Denki Seizo K.K. Ltd. are installed in all four wheels as the driving powertrain. Table II shows the specifications of the in-wheel motors. Because this motor adopts a direct drive system, the reaction force from the road is directly transferred to the motor without gear reduction and backlash. This vehicle is therefore ideal for studying the developed estimation and control methods. Fig. 3 shows the front and rear in-wheel motors.

III. VEHICLE MODELING

A. Longitudinal motion equation and slip ratio

In this section, the equations of vehicle dynamics are explained. As shown in Fig. 4, the equation of the rotational motion of each wheel can be given as

$$J_{ij}\dot{\omega}_{ij} = T_{ij} - T_{bij} - rF_{dij}, \quad (1)$$

where J is the wheel inertia; ω , the wheel angular velocity; T , the motor torque; T_b , the mechanical brake torque; r ,

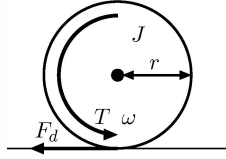


Fig. 4. Rotation of wheel.

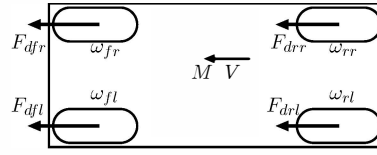


Fig. 5. Variables in vehicle motion.

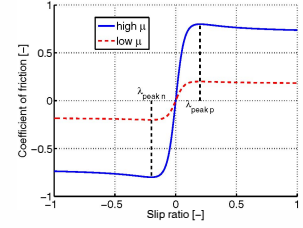


Fig. 6. Typical μ - λ curve.

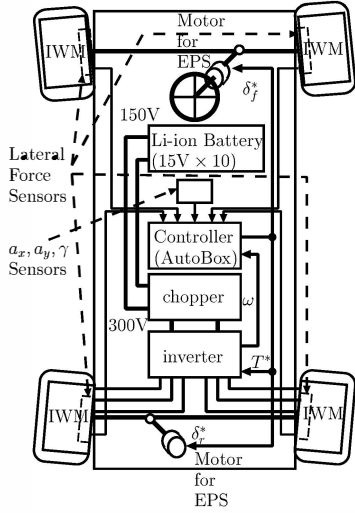


Fig. 2. Configuration of experimental vehicle.

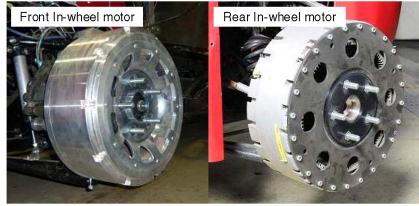


Fig. 3. In-wheel motors.

Table II
SPECIFICATIONS OF IN-WHEEL MOTOR.

	Front	Rear
Manufacturer	TOYO DENKI	
Type	Direct drive system Outer rotor type	
Rated torque	110 [Nm]	137 [Nm]
Maximum torque	500 [Nm]	340 [Nm]
Rated power	6.0 [kW]	4.3 [kW]
Maximum power	20.0 [kW]	10.7 [kW]
Maximum speed	1113 [rpm]	1500 [rpm]
Weight	32 [kg]	26 [kg]
Cooling system	Air cooling	

the wheel radius; and F_d , the driving force at the point at which the wheel makes contact with the ground. In addition, i and j are indices for f/r (front/rear) and l/r (left/right), respectively. The equation of longitudinal motion of the vehicle body shown in Fig. 5 is given as

$$M\dot{V} = F_{dfl} + F_{dfr} + F_{drl} + F_{drr} - F_{dr}, \quad (2)$$

where M is the vehicle mass; V , the vehicle velocity; and F_{dr} , the driving resistance. When the vehicle accelerates or decelerates, the wheel velocity $V_\omega = r\omega$ differs from

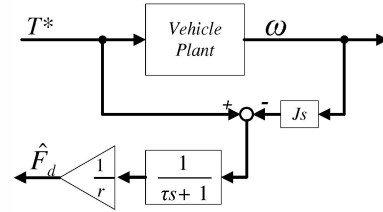


Fig. 7. Driving force observer.

the vehicle velocity V . The slip ratio λ is defined as

$$\lambda = \frac{V_\omega - V}{\max(V_\omega, V, \epsilon)}, \quad (3)$$

where ϵ is a tiny value to prevent division by zero. The driving force F_d and the driving stiffness D_s at each wheel are respectively obtained as

$$F_{dij} = \mu_{ij} N_{ij}, \quad (4)$$

$$D_{sij} = \left. \frac{dF_{dij}}{d\lambda_{ij}} \right|_{\lambda_{ij}=0}, \quad (5)$$

where N is the normal reaction force on each wheel and μ , the friction coefficient.

The relationship between μ and λ depends on the road condition, and it is given as shown in Fig. 6 [10]. There are two peaks at $\lambda_{\text{peak,p}}$ and $\lambda_{\text{peak,n}}$, where μ takes the maximum and the minimum value, respectively. In the domain of $\lambda_{\text{peak,n}} \leq \lambda \leq \lambda_{\text{peak,p}}$, μ is a monotonically increasing function of λ , and outside this domain, it is a monotonically decreasing function.

B. Driving force observer

In (1), the motor torque is calculated from the motor current. Moreover, $\dot{\omega}$ can also be calculated. Therefore, the driving force can be estimated by using the driving force observer (DFO)[1] based on (6).

$$\hat{F}_{dij} = \frac{1}{r} (T - J\dot{\omega}) \quad (6)$$

The block diagram of DFO is shown in Fig. 7.

IV. SLIP RATIO ESTIMATION AND CONTROL METHOD WITHOUT VEHICLE VELOCITY

Our group has proposed a slip ratio estimation and control method without the detection of vehicle velocity when the vehicle is accelerating and decelerating in [7] and [11], respectively.

As shown in Fig. 6, the friction coefficient between the tire and the road becomes minimum near -0.2, and the maximum brake torque is obtained. Therefore, the

braking distance becomes shorter if the wheel velocities are controlled to have an optimum slip ratio.

First, the slip ratio estimation method without vehicle velocity is explained. Next, the slip ratio control method is explained.

A. Slip ratio estimation

In this section, the equation for slip ratio estimation is derived. The form of the equation differs depending on whether the vehicle is accelerating or decelerating.

First, the equation for acceleration is derived. By substituting from (1) and (2) into the time derivative of (3) for acceleration ($V_\omega > V$), the state equation for λ is obtained as

$$\dot{\hat{\lambda}}_{ij} = \frac{\dot{\omega}_{ij}}{\omega_{ij}}(1 - \hat{\lambda}_{ij}) - \frac{T_m - T_b - J_\omega \dot{\omega} - r\hat{F}_{dr}}{r^2 M \omega_{ij}}, \quad (7)$$

where T_m , T_b , and $J_\omega \dot{\omega}$ are respectively given as follows:

$$T_m = T_{fl} + T_{fr} + T_{rl} + T_{rr}, \quad (8)$$

$$T_b = T_{bfl} + T_{bfr} + T_{brl} + T_{brr}, \quad (9)$$

$$J_\omega \dot{\omega} = J_{fl} \dot{\omega}_{fl} + J_{fr} \dot{\omega}_{fr} + J_{rl} \dot{\omega}_{rl} + J_{rr} \dot{\omega}_{rr}. \quad (10)$$

As shown in III-B, F_d can be estimated from the DFO. If the driving resistance \hat{F}_{dr} is not negligibly small, it can be obtained from the accelerometer signal a_x and \hat{F}_d based on (2). Then, we can assume that $\hat{F}_d = F_d$. The motor torque, mechanical brake torque, and rotation speed of the motor are obtained from the motor current, brake line pressure, and resolver attached to the motor, respectively.

To analyze the convergence of the estimated value, the estimation error is defined as $e(t) = \lambda_{ij} - \hat{\lambda}_{ij}$. Then, the following equation is obtained for the estimation error:

$$\frac{d}{dt}e(t) = -\frac{\dot{\omega}_{ij}}{\omega_{ij}}e(t) + \frac{F_{dr} - \hat{F}_{dr}}{rM\omega_{ij}}. \quad (11)$$

By the abovementioned assumption, $F_{dr} - \hat{F}_{dr}$ is negligible. Then, the estimation error converges to zero when $\dot{\omega} > 0$ because the vehicle is moving forward ($\omega > 0$). When the vehicle is accelerating, $\dot{\omega}$ is positive almost all the time. $\dot{\omega}$ rapidly becomes negative when the vehicle recovers adhesion after slipping.

Next, the equation for deceleration is derived. As in the case of acceleration, the equation for slip ratio estimation for deceleration is defined as

$$\dot{\hat{\lambda}}_{ij} = \frac{\dot{\omega}_{ij}}{\omega_{ij}}(1 + \hat{\lambda}_{ij}) - \frac{T_m - T_b - J_\omega \dot{\omega} - r\hat{F}_{dr}}{r^2 M \omega_{ij}}(1 + \hat{\lambda}_{ij})^2. \quad (12)$$

The estimation error for deceleration ($e(t) = \lambda_{ij} - \hat{\lambda}_{ij}$) is dominated by the following equation:

$$\frac{d}{dt}e(t) = \left\{ \frac{\dot{V}_{\omega_{ij}}}{V_{\omega_{ij}}} - \frac{\dot{V}}{V_{\omega_{ij}}}(2 + \lambda_{ij} + \hat{\lambda}_{ij}) \right\} e(t). \quad (13)$$

Then, the estimation error converges to zero when (14) is satisfied.

$$\dot{V}_{\omega_{ij}} - \dot{V}(2 + \lambda_{ij} + \hat{\lambda}_{ij}) < 0 \quad (14)$$

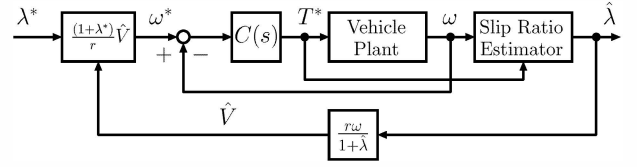


Fig. 9. Block diagram of slip ratio control during deceleration.

Here, the range of slip ratio λ is $-1 < \lambda < 0$. Therefore, this estimation error surely converges to zero when the deceleration of the wheel is at least twice as large as that of the vehicle. This means that the wheel is slipping. Then, both λ_{ij} and $\hat{\lambda}_{ij}$ approach -1.0. Then, (14) is satisfied all the time. Once the estimation error converges to zero, the slip ratio can continue to be estimated accurately.

Fig. 8 shows the simulation and experiment result for slip ratio estimation during deceleration. The real value of the slip ratio is calculated based on (3). The value of the vehicle velocity is obtained using an optical sensor that is used only for the evaluation of slip ratio estimation. Fig. 8(a) and Fig. 8(c) show the performance of slip ratio estimation. The estimated slip ratio tracks the real value in both figures.

B. Slip ratio control

Next, the slip ratio control with wheel velocity control is designed, as shown in Fig. 9. Because the wheel velocity can be detected using the resolver, the estimation of the slip ratio is equivalent to the estimation of the vehicle velocity. The estimated vehicle velocity can be calculated from (3) based on the estimated slip ratio. Then, when the vehicle accelerates, the reference value of the wheel angular velocity at the optimum slip ratio is calculated from (15).

$$\hat{V} = r\omega(1 - \hat{\lambda}), \quad \omega^* = \frac{\hat{V}}{r(1 - \lambda^*)}. \quad (15)$$

Similarly, the reference value of the wheel angular velocity during deceleration is calculated from (16)

$$\hat{V} = \frac{r\omega}{1 + \hat{\lambda}}, \quad \omega^* = \frac{1 + \lambda^*}{r} \hat{V}. \quad (16)$$

By using the reference value of the wheel velocity calculated by (15) or (16), slip ratio control is achieved by wheel velocity control. A simple proportional-integral (PI) controller is designed as the wheel velocity controller, where the nominal plant is assumed as

$$\omega = \frac{1}{J_\omega s} T, \quad (17)$$

and the closed-loop pole is located at -30 rad/s with the pole placement method and the target slip ratio is -0.2.

The effectiveness of slip ratio control during deceleration is verified through a simulation and experiments. The vehicle decelerated only with the rear wheels both without and with control. Fig. 10 shows the simulation and experimental results of slip ratio control.

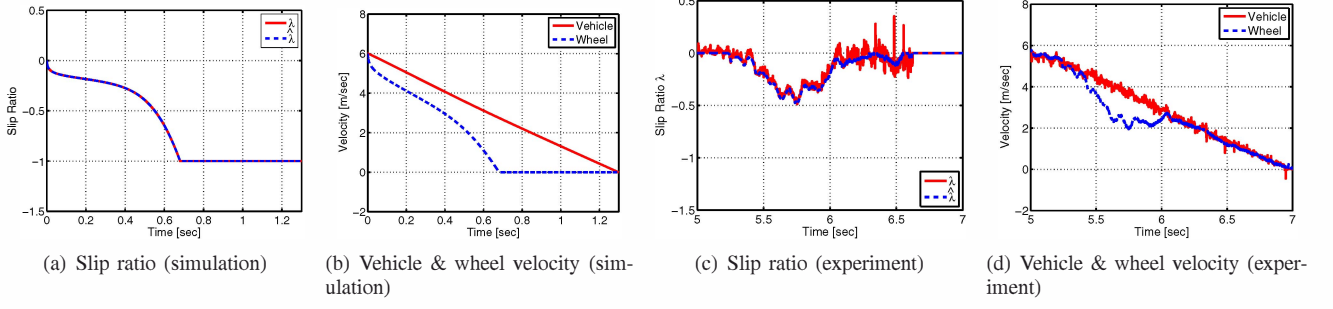


Fig. 8. Simulation and experimental results of slip ratio estimation.

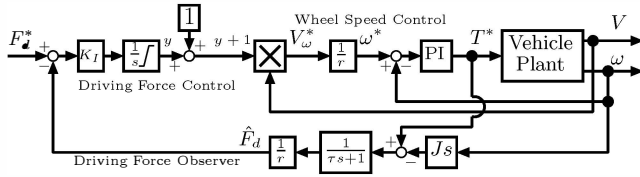


Fig. 11. Block diagram of DFC based on wheel velocity control.

Fig. 10(a) and Fig. 10(c) indicate that the wheels do not lock and that the slip ratio converges to the target of -0.2 successfully.

V. DRIVING FORCE CONTROL BASED ON WHEEL VELOCITY CONTROL

A. Summary of driving force control based on wheel velocity control

Slip ratio control can achieve the maximum driving force on a slippery road if the slip ratio reference is set to an optimal value. However, it is difficult to select the correct reference value. Therefore, the DFC method was proposed in [8]. The block diagram of DFC is shown in Fig. 11. The outer loop is the control loop of the driving force based on the DFO, and the inner loop is the wheel velocity loop that controls the slip ratio. F_d^* is the driving force reference and \hat{F}_d is the estimated driving force.

This method achieves a driving force reference even on a low μ road. If the driving force reference is too large to realize, this method achieves the maximum allowable driving force with respect to the road condition.

Because the definition of slip ratio λ differs for acceleration ($V_\omega \geq V$) and deceleration ($V_\omega < V$), λ is unsuitable for use as a control reference. Therefore, instead of the slip ratio, the control input y , defined as follows, is controlled.

$$y = \frac{V_\omega}{V} - 1. \quad (18)$$

This is the same definition as the definition of slip ratio for deceleration. The relationship between λ and y in the domain of $\lambda > 0$ is calculated as

$$y = \frac{\lambda}{1 - \lambda}, \quad (19)$$

indicating that y equals λ when $|\lambda| \ll 1$ and that they always have one-to-one correspondence.

From (18), the wheel velocity reference V_ω^* of the inner loop is calculated as

$$V_\omega^* = (1 + y)V, \quad (20)$$

indicating that the vehicle cannot start moving when at rest ($V = 0$) because V_ω^* is equal to 0 independently of y . To prevent this problem, the reference V_ω^* is modified, where V is smaller than a given constant σ , as shown in (21).

$$\begin{cases} V_\omega^* = V + y\sigma & (V < \sigma), \\ V_\omega^* = V + yV & (V \geq \sigma). \end{cases} \quad (21)$$

A saturation function is applied to the integrator output for limiting y to $y_{\min} \leq y \leq y_{\max}$. With this saturation, traction can be retained by keeping the slip ratio within the domain where μ is a monotonic function of λ .

B. Verification through simulation and experiments

The effectiveness of DFC is verified through simulation and experiments. The vehicle runs on a high μ road for 2 [s], then on a low μ road for 2 s, and again on a high μ road.

The experimental vehicle starts at the start point and accelerates with driving force reference $F_d^* = 600$ [N] for each front wheel. The parameters are $K_I = 0.01$, $\tau = 30$ [ms], and $y_{\max} = 0.25$, which corresponds to a slip ratio of $\lambda = 0.2$. The wheel velocity PI controller is designed by the pole assignment method for the nominal plant $\frac{1}{Js}$ with the pole at -20 rad/s.

Fig. 12 and Fig. 13 respectively show the simulation and experimental results of DFC. From Fig. 12(a) and Fig. 13(a), the driving force converges to the reference on a high μ road. In addition, from Fig. 12(c) and Fig. 13(c), the wheels do not slip and the slip ratio keeps the set value λ_{peak} on a low μ road.

VI. DRIVING FORCE DISTRIBUTION METHOD FOR INSTANTANEOUS SLIPPERY ROADS

A. Cost function for driving force distribution

In this section, the driving force distribution method for instantaneous slippery roads is explained. When the control input y of DFC approaches the upper limit, the driving force is saturated and reduced. To avoid this reduction, y of each wheel needs to be sufficiently small

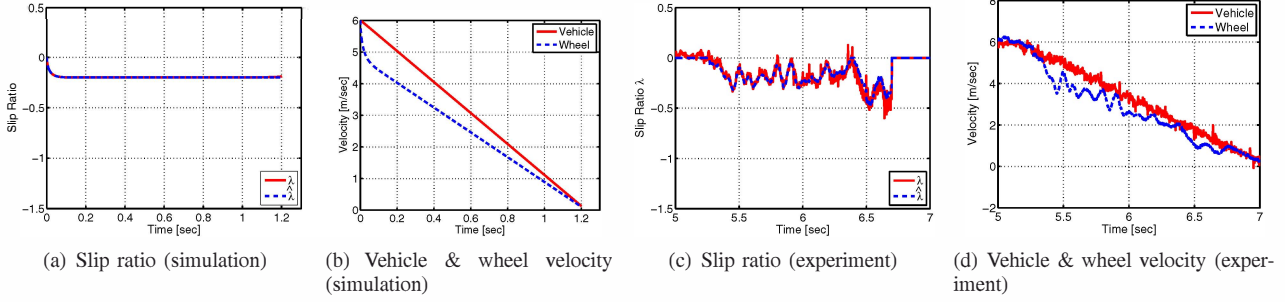


Fig. 10. Simulation and experimental results of slip ratio control.

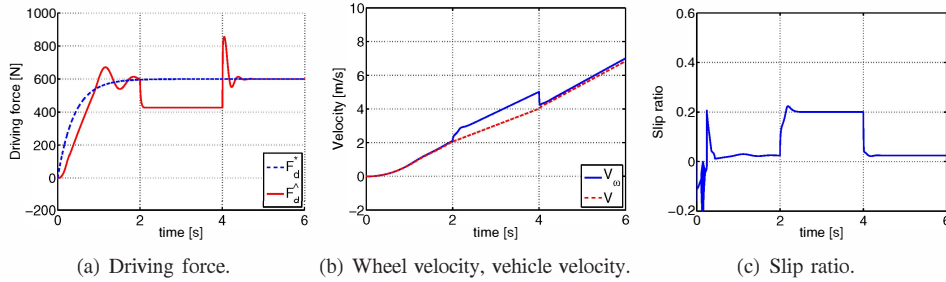


Fig. 12. Simulation result (driving force control based on wheel velocity control).

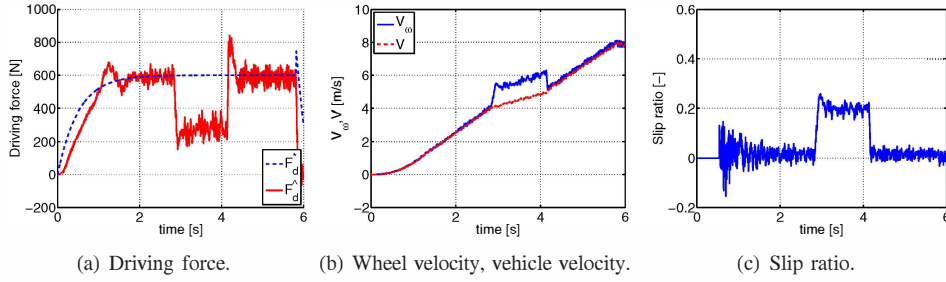


Fig. 13. Experimental result (driving force control based on wheel velocity control).

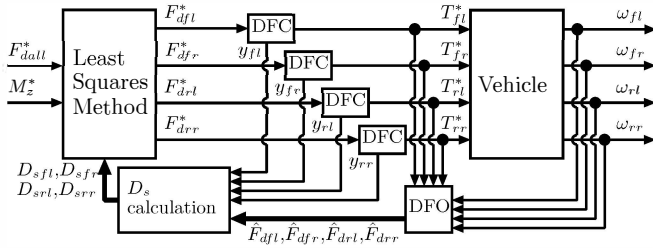


Fig. 14. Block diagram of driving force distribution method.

to prevent saturation. Therefore, [8] proposed a novel method to generate the driving force reference to minimize y of each wheel while satisfying the total driving force reference F_{dall}^* and yaw-moment reference M_z^* that is generated by the driving force difference between the left and the right in-wheel motors.

The relationship between the driving force of each wheel

F_{dij} , F_{dall} , and M_z is given as follows:

$$\begin{bmatrix} 1 & 1 & 1 & 1 \\ -\frac{d_f}{2} & \frac{d_f}{2} & -\frac{d_r}{2} & \frac{d_r}{2} \end{bmatrix} \begin{bmatrix} F_{dfl} \\ F_{dfr} \\ F_{drl} \\ F_{drr} \end{bmatrix} = \begin{bmatrix} F_{dall} \\ M_z \end{bmatrix}. \quad (22)$$

Here, by setting the coefficient matrix in the left-hand side as \mathbf{A} , the vector of the driving force of each wheel $[F_{dfl}, F_{dfr}, F_{drl}, F_{drr}]^T$ as \mathbf{x} , and the vector of the total driving force and yaw moment $[F_{dall}, M_z]^T$ as \mathbf{b} , (22) can be rewritten as $\mathbf{Ax} = \mathbf{b}$. From (5), the driving stiffness of each wheel D_{sij} can be obtained as

$$D_{sij} = \frac{F_{dij}}{y_{ij}}. \quad (23)$$

Then, the cost function J is defined as the sum of squares of the DFC inputs y_{ij} .

$$\begin{aligned} J &= y_{fl}^2 + y_{fr}^2 + y_{rl}^2 + y_{rr}^2 \\ &= \frac{F_{dfl}^2}{D_{sfl}^2} + \frac{F_{dfr}^2}{D_{sfr}^2} + \frac{F_{drl}^2}{D_{srl}^2} + \frac{F_{drr}^2}{D_{srr}^2}. \end{aligned} \quad (24)$$

Therefore, the weighted least-squares solution \mathbf{x}_{opt} of (22) that minimizes J and the weighting matrix \mathbf{W} are given

as follows.

$$\mathbf{x}_{opt} = \mathbf{W}^{-1} \mathbf{A}^T (\mathbf{A} \mathbf{W}^{-1} \mathbf{A}^T)^{-1} \mathbf{b}, \quad (25)$$

$$\mathbf{W} = \text{diag} \left(\frac{1}{D_{sfl}^2}, \frac{1}{D_{sfr}^2}, \frac{1}{D_{srl}^2}, \frac{1}{D_{srr}^2} \right). \quad (26)$$

Fig. 14 shows the block diagram of the entire system. The driving force references F_{dij}^* are given by \mathbf{x}_{opt} , and the driving stiffness of each wheel D_{sij} is calculated by the following equation.

$$D_{sij} = \frac{\hat{F}_{dij}}{y_{ij}}, \quad (27)$$

where \hat{F}_{dij} is the estimated driving force of each wheel. Lower limitations 0.005 and 50 are imposed on y_{ij} and \hat{F}_{dij} in (26), respectively, to avoid division by zero for both in (27).

B. Experiment on instantaneous slippery road

In this section, simulation and experimental results of acceleration on an instantaneous slippery road are presented. An extremely low μ road of length 0.9 [m], shorter than the wheel base of "FPEV2-Kanon," is set at a distance of 2.0 m from the start point. A polymer sheet is used as the slippery road. This sheet, referred to as a low- μ sheet in this study, can be watered to realize a low μ road with $\mu = 0.2$.

The experimental vehicle starts at the start point and accelerates with total driving force reference $F_{dall}^* = 600/r = 1993.4$ [Nm]. The front and rear motor torque is respectively limited to 300 and 220 Nm to ensure safety inside the university. The parameters are $K_I = 0.01$, $\tau = 30$ [ms], and $y_{max} = 0.25$, which corresponds to a slip ratio of $\lambda = 0.2$. The wheel velocity PI controller is designed by the pole assignment method for the nominal plant $\frac{1}{s}$ with the pole at -20 rad/s. All parameters are the same for each wheel.

The experimental results with only DFC are shown in Fig. 15 and those with driving force distribution are shown in Fig. 16. With only DFC, although traction is obtained as shown in Fig. 15(a), the driving force decreases as shown in Fig. 15(b) and Fig. 15(c).

In contrast, with the proposed method, Fig. 16(b) shows that the driving force on each wheel is distributed to retain the total driving force as shown in Fig. 16(c) as well as the traction as shown in Fig. 16(a). In addition, Fig. 16(d) shows that the proposed method prevents the saturation of y .

VII. DIRECT DRIVING FORCE CONTROL BASED ON DRIVING STIFFNESS ESTIMATION

A. Direct driving force control

DFC explained in V has limitations in the control bandwidth caused by the delay in the DFO and multiple control loops (e.g., DFC loop, wheel velocity loop, and current loop). Therefore, the DDFC method was proposed in [9]. This control system is designed based on a 2 degree of freedom control methodology. The feedforward (FF)

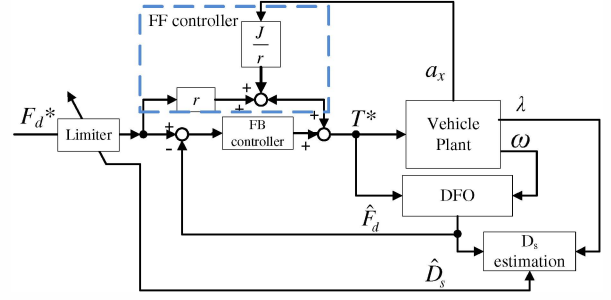


Fig. 17. Block diagram of direct driving force control.

controller is mainly used to improve the control bandwidth. The feedback controller suppresses the disturbance and the modeling error. The driving force is not measurable. Therefore, it is estimated using the DFO. The block diagram of the proposed method is shown in Fig. 17.

B. DDFC controller design

From (1) and $r\omega = V$, the driving force reference is achieved by the torque reference on a high μ road and is represented by

$$T_{ff}^* = rF_d^* + J\frac{\dot{V}}{r}, \quad (28)$$

where T_{ff}^* is the motor torque reference from the FF controller. By using this torque reference, the inertial torque on a high μ road can be compensated and the sudden increase in the inertial torque can be suppressed on a slippery road.

The gain of the feedback (FB) controller is determined by the pole placement method with the following nominal plant.

$$F_d = \frac{1}{r + \frac{J}{rM(1-\lambda)}} T. \quad (29)$$

By using this model, the gain of controller can be designed. Thus, the FB signal is used to estimate the driving force by the DFO.

C. Traction control based on reference limitation

The FF controller mentioned in section VII accelerates the slipping wheel when the driving force reference exceeds the maximum driving force on the low μ road.

Then, traction control is achieved by using a limiter on the driving force reference. The value of the maximum driving force is calculated by multiplying the estimated driving stiffness \hat{D}_s and optimal slip ratio λ_{peak} . The range of limitation is set at the estimated maximum driving force.

$$\begin{cases} F_{d \max} = \hat{D}_s \lambda_{peak p}, \\ F_{d \min} = \hat{D}_s \lambda_{peak n}. \end{cases} \quad (30)$$

In this study, $\lambda_{peak p}$ and $\lambda_{peak n}$ are treated as known values, and their value is set to ± 0.2 .

Here, the value of the driving stiffness can be estimated by applying the recursive least-squares algorithm (RLS) using the forgetting factor on λ and \hat{F}_d . The details of D_s estimation are described in [12].

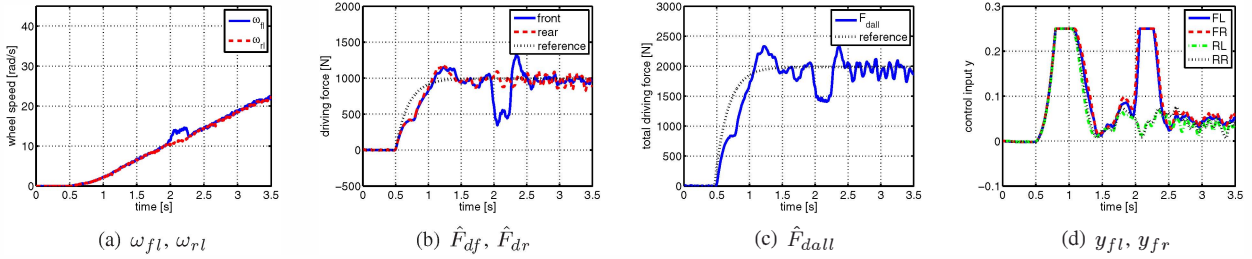


Fig. 15. Experiment of instantaneous slippery road (only DFC).

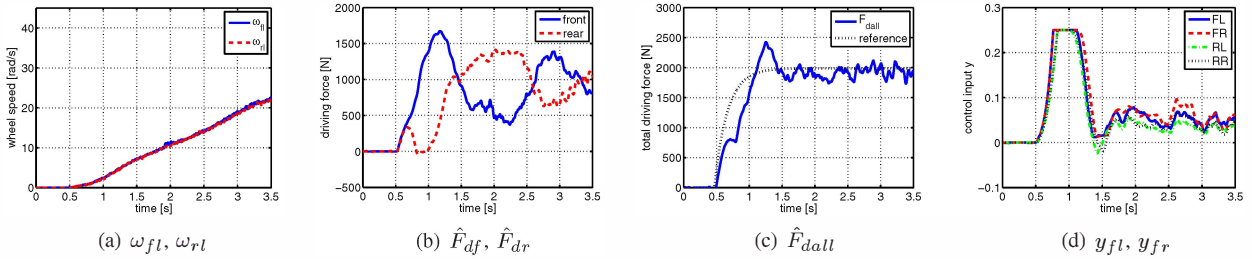


Fig. 16. Experiment of instantaneous slippery road (with driving force distribution).

D. Simulation of DDFC

A simulation is carried out to verify the effectiveness of the proposed method, i.e., DFC based on driving stiffness estimation. The maximum value of the friction coefficient μ_{peak} is set to 0.8 on a high μ road and 0.2 on a low μ road. λ_{peak} is set as 0.2.

The closed-loop pole used in the pole placement design of the FB controller is -3 rad/s. The driving force reference is a step response of the first-order lag system. The size of the step is set to 450[N]. The vehicle travels on a high μ road for 2 s, then goes to a low μ road for 2 s, and then goes on a high μ road again.

The parameters used in D_s estimation are as follows: minute slip ratio used in conditional updating [13], $\varepsilon_\lambda = 0.01$; forgetting factor, $\rho = 0.95$; and sampling time, $T_s = 1$ [ms]. When the vehicle moves slowly, the calculated slip ratio becomes too large. Therefore, the updating of D_s estimation starts if the condition $V > 0.1$ [m/s] is satisfied.

Fig. 18 shows the simulation result of DFC considering the inertial torque term. As shown in Fig. 18(a), there is no error in the driving force for a high μ road. Therefore, by considering the inertial torque, DFC is achieved by the FF controller on a high μ road.

Moreover, the tire slip is reduced as shown in Fig. 18(b) and 18(c). The slip ratio keeps the target optimal slip ratio λ_{peak_p} on a low μ road. Therefore, the maximum driving force output is achieved by setting λ_{peak_p} to an optimal value.

E. Experiment of DDFC

In this section, the effectiveness of the DDFC method is verified through experiments. The vehicle travels from a high μ road to a low μ road. The abovementioned polymer sheet is used as the slippery road.

In this experiment, only the front wheels are driven. Then, the vehicle speed is measured by the wheel velocity of the non-drive wheels. This vehicle velocity is used to calculate the slip ratio λ . The parameters used in D_s estimation are the same as in the simulation.

Here, the plotted slip ratio value changes to zero when $V < 0.2$ [m/s] because the reliability of the slip ratio is low when the vehicle velocity is low.

The trends of the experimental results are the same as those of the simulation results. From Fig. 19(a), the effect of the compensation of the inertial term is confirmed. In addition, 19(c) shows that traction control is successfully achieved by employing the reference limiter.

VIII. CONCLUSION

In this paper, we review our recent studies on traction control for EVs with in-wheel motors. First, estimation and control methods for the slip ratio without the detection of vehicle speed are explained. Second, DFC and driving force distribution method are explained. Finally, DFC is improved without using the inner-loop controller of the wheel velocity.

ACKNOWLEDGMENT

This research was partly supported by an Industrial Technology Research Grant Program from the New Energy and Industrial Technology Development Organization (NEDO Project ID: 05A48701d). Additionally, this work was supported by MEXT KAKENHI grant number 22246057.

REFERENCES

- [1] Y.Hori, "Future vehicle driven by electricity and control-research on four-wheel-motored: UOT electric march II", *IEEE Trans. IE*, Vol.51, No. 5, 2004
- [2] S.Murata, "Vehicle dynamics innovation with in-wheel motor", In *Proceedings 1st International Electric Vehicle Technology Conference*, no. 20117204, 2011

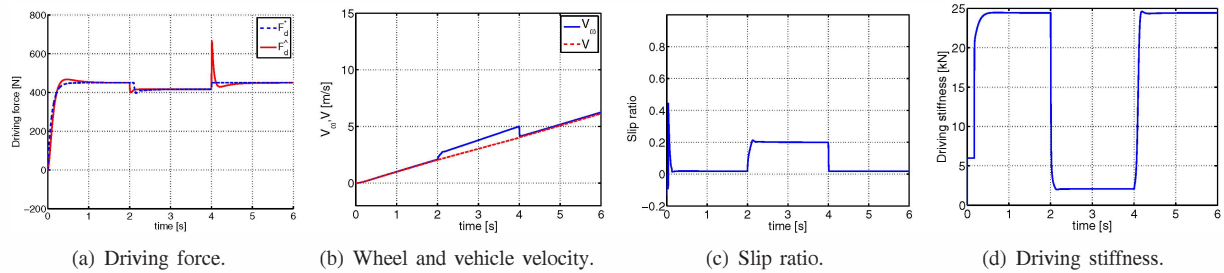


Fig. 18. Simulation result (direct driving force control).

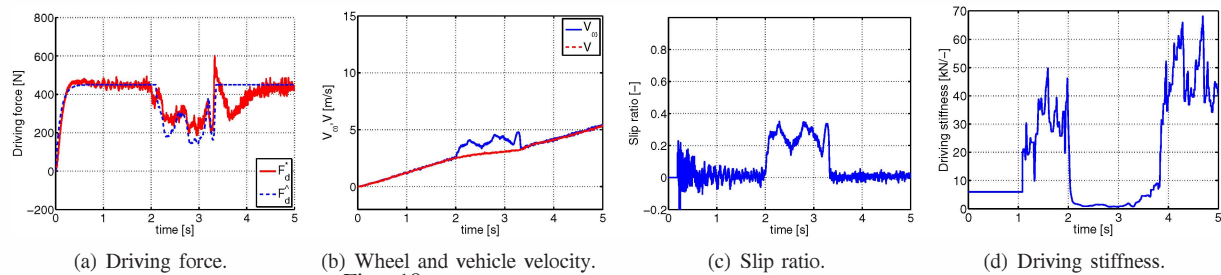


Fig. 19. Experimental result (direct driving force control).

- [3] K.H.Lee, J.H.Bak and C.H.Lee: "Study on active steering control of vehicle for safe driving in highway with GPS information", In *Proc. Intelligent Vehicles Symposium (IV)*, pp.554–557, 2012
- [4] B.Subudhi and S.S.Ge: "Sliding-mode-observer-based adaptive slip ratio control for electric and hybrid vehicles", *IEEE Transactions on Intelligent Transportation Systems*, Vol. PP, Issue 99, pp.1–10, 2012
- [5] M.S.Geamanu, A.Cela, G.LeSollic, H.Mounier and S.Niculescu: "Road condition estimation and longitudinal control for electric vehicles", In *Proc. the 11th International Conference on Control, Automation and Systems*, pp. 599–604, 2011
- [6] D.Foito, M.Guerreiro and A.Cordeiro: "Anti-slip wheel controller drive for EV using speed and torque observers", In *Proc. the 18th International Conference on Electrical Machines*, pp. 1–5, 2008
- [7] T.Suzuki and H.Fujimoto: "Slip ratio estimation and regenerative brake control without detection of vehicle velocity and acceleration for electric vehicle at urgent brake-turning", In *Proc. The 11th IEEE International Workshop on Advanced Motion Control Proceedings*, Niigata, pp.273–278, 2010
- [8] K.Maeda, H.Fujimoto and Y.Hori: "Four-wheel driving-force distribution method for instantaneous or split slippery roads for electric vehicle with in-wheel motors", In *Proc. The 12th International Workshop on Advanced Motion Control*, Sarajevo, Bosnia and Herzegovina, pp.1–6, 2012.
- [9] J. Amada and H. Fujimoto: "Torque based direct driving force control method with driving stiffness estimation for electric vehicle with in-wheel motor", In *Proc. The 38th Annual Conference of the IEEE Industrial Electronics Society*, Montreal, Canada, 2012 (accepted)
- [10] H.B.Pacejka and E.Bakker: "The magic formula tyre model", Tyre models for vehicle dynamic analysis: In *Proc. the 1st International Colloquium on Tyre Models for Vehicle Dynamics Analysis*, held in Delft, The Netherlands (1991)
- [11] K.Fujii, H.Fujimoto, M.Kamachi and H.Yoshida: "Experimental verification of traction control for electric vehicle based on slip ratio estimation without vehicle speed detection", *JSAE Review of Automotive Engineers*, Vol. 29, pp. 369–372, 2008 (invited)
- [12] T.Kanou and H.Fujimoto, "Slip-ratio based yaw-rate control with driving stiffness identification for electric vehicle", In *9th International Symposium on Advanced Vehicle Control*, Japan, pp. 786–791, 2008
- [13] H.Fujimoto and B.Yao, "Multirate adaptive robust control for discrete-time non-minimum phase systems and application to linear motors", *IEEE/ASME Trans. Mechatronics*, Vol.10, No.4, pp.371–377, 2005